36th AIAA Plasma Dynamics and Laser conference, 06-09 Jun 2005, Toronto, Canada

Two-dimensional Fluid Model of DC and RF Plasma Discharges in Magnetic Field

Haribalan Kumar* and Subrata Roy†

Computational Plasma Dynamics Laboratory, Kettering University, Flint, Michigan 48504

The hydrodynamic equations of continuity and momentum for electrons and ions along with the electrostatic field equation are solved numerically using a self-consistent finite-element algorithm in the low-pressure, high frequency regime. The plasma formation over a flat plate is investigated for three different cases. The two-dimensional numerical algorithm is first benchmarked with published literature for plasma formed between symmetric electrodes in nitrogen gas. Discharge characteristics of plasma for an electrode-insulator configuration are then analyzed under steady and transient conditions using argon as a working gas. The effect of magnetic field on electric potential and charge difference is studied for an infinitesimally thin electrode. The magnetic field distorts the stream-wise distribution because of strong y-momentum v×B coupling. Finally, the shape effects of insulator-conductor edge for an electrode of finite thickness have been compared using a 90° shoulder and a 45° chamfer. The 90° chamfer displays a stronger body force created due to plasma in the downward and forward directions.

Nomenclature

α	Ionization coefficient, cm^{-1}
B	Magnetic field, Tesla
d	Characteristic length, cm
D	Diffusion coefficient, cm^2/s
e	Electron charge, statcoulomb
ε	Permittivity, $C^2/N.m^2$
E	Electric field, V/cm
Γ	Flux, cm^{-2}/s
J	Jacobian
k	Boltzman constant, J/K
λ_{De}	Electron debye length, cm
μ	Mobility, $cm^2V^{-1}s^{-1}$
n(N)**	Number density, cm^{-3}
p	Pressure, torr
$\varphi(\Phi)$	Potential, V
S_w	Sheath thickness, cm
$t(\tau)$	Time co-ordinate, s
T	Temperature, eV
V(u)	Species hydrodynamic velocity, cm/s
ω	Applied frequency, sec^{-1}
x, y	Spatial co-ordinates, cm
Ω	Computational domain
∇	Gradient

** Terms appearing within braces are normalized variables

Subscripts:

B	Bohm
e	Electron
i	Ion
0	Reference value

* Graduate Research Assistant, kuma6164@kettering.edu. 1700 West Third Ave, and AIAA Student Member.
† Associate Professor of Mechanical Engineering, sroy@kettering.edu. 1700 West Third Ave, AIAA Associate Fellow.

I. INTRODUCTION

THE increasing application of plasma in aerospace community demands supporting theories to quantify and explain experimental observations. Particularly, with growing interest in plasma based flow control techniques, there is a necessity to predict the plasma discharge characteristics effectively. Thus, a time accurate and geometry versatile numerical tool would prove useful in accurately calculating the discharge characteristics and its electrodynamic effects. The present effort is focused towards modeling and simulation of a two-dimensional plasma discharge formed in the high frequency, low-pressure regime.

The dynamics of sheath in one dimension in the low and intermediate pressure regime have been studied in literature from numerical simulations[1-5]. Boeuf and Pitchford[6], Dalvie[7] et. al and Passchier and Godheer[8] simulated argon discharge for cylindrical geometry in two dimensions. Kim and Economou[9] investigated plasma formation over an inhomogeneous flat wall. Recent efforts have also considered effect of external electromagnetic force on plasma wall interaction[10-11]. In these simulations, fluid and/or PIC formulation was used to model the system. Fluid equations are based on conservation laws derived from moments of Boltzmann equation while particle approaches like PIC/MC involves plasma characterization by following millions of computational particles for each species. The numerical advantage of using fluid descriptions is obvious for treating high-density plasma in which methods like PIC become prohibitively expensive. Inspite of these earlier attempts, the capability to simulate characteristics of a discharge in the presence of electric and magnetic fields remain limited.

To contribute to this growing need, we present a two dimensional hydrodynamic plasma model with electric and applied magnetic fields. A high-fidelity finite-element procedure anchored in the Multi-scale Ionized Gas (MIG) flow code[12-14] is implemented to simulate the plasma using fluid description. The axial and transverse nature of resulting electrostatic field, forces and charge difference are investigated. The MIG code employs a self-consistent approach to model the near wall physics of plasma gas interactions. In a self-consistent plasma-wall model followed in many earlier works[7,9,11-14], the space charge effect is incorporated for the entire region. The sheath structure is analyzed in the post-processing phase unlike the patching and matching techniques where bulk plasma forms a boundary condition to sheath solution.

First we report the transient nature of plasma formed between symmetric electrodes in one-dimension. The study is extended in two dimensions to investigate the plasma dynamics under steady and transient conditions over a flat plate for three different cases. The numerical algorithm is first benchmarked with published literature for nitrogen gas plasma formed between symmetric electrodes. Discharge characteristics of plasma for an infinitesimally thin electrode configuration are then analyzed under applied DC and RF potentials using argon as a working gas. Finally, the shape effect for an electrode of finite thickness is considered for a 90^o shoulder and a 45^o chamfer.

The paper is organized as follows. Section II describes the problem specifications and identifies the hydrodynamic equations. Section III explains the methodology adopted to solve the system of equations. Section IV describes and interprets the results obtained for the discharge in one and two-dimensional discharge configurations. Section V summarizes the conclusions.

II. CONTINUUM MODEL

The unsteady transport for electrons and ions are derived from fluid dynamics in the form of mass and momentum conservation equations. The species momentum is modeled by the drift-diffusion equation under isothermal conditions. Here, the flux is written in terms of species transport coefficients by neglecting inertial acceleration in the collisional regime. Electron temperature (T_e) is of the order of ~11,600K (1 eV) and ions are assumed cold at ~300 K (0.026 eV). The continuity equation for ion and electron number densities is given by

$$\frac{\partial n_i}{\partial t} + \nabla.(n_i \boldsymbol{V}_i) = \alpha \left|\Gamma_e\right| \qquad \left|\Gamma_e\right| = \sqrt{\left(n_e V_e\right)_x^2 + \left(n_e V_e\right)_y^2} \qquad (1)$$

$$\frac{\partial n_e}{\partial t} + \nabla.(n_e \boldsymbol{V}_e) = \alpha \left|\Gamma_e\right|$$

where n is the number density and V is the species hydrodynamic velocity. As the sheath is collision dominated, electrons are not assumed to follow Maxwellian distribution. All electrochemical data provided here are for argon, which is the working gas for all cases except for a benchmark case for which nitrogen gas data have been used from Ref 10. For a pressure of 0.1 Torr, electron-ion recombination ~$2\text{x}10^{-12}$ cm^3/s and has negligible effect on mass balance[6,15]. The discharge is maintained using a Townsend ionization scheme resulting in production of charge through impact ionization. The ionization rate is usually expressed as function of electron drift velocity and Townsend coefficients[6,16-17].

The Townsend coefficient, α appearing in Eqn (1) is given by

$$\alpha = Ape^{-B/(|\boldsymbol{E}|/p)} \tag{2}$$

where $A = 34\ \text{cm}^{-1}.\text{Torr}^{-1}$ *and* $B = 16\ \text{V/(cm.Torr)}$ are pre-exponential and exponential constants, respectively. $|\Gamma_e|$ is the effective electron flux. The electronic and ionic flux in (1) are written as

$$n_i \boldsymbol{V}_i = n_i \mu_i (\boldsymbol{E} + \boldsymbol{V}_i \times \boldsymbol{B}_z) - D_i \nabla n_i \tag{3}$$

$$n_e \boldsymbol{V}_e = -n_e \mu_e (\boldsymbol{E} + \boldsymbol{V}_e \times \boldsymbol{B}_z) - D_e \nabla n_e \tag{4}$$

where the electrostatic field given by $\boldsymbol{E} = -\nabla\varphi$. $\boldsymbol{V}$x$\boldsymbol{B}$ is the Lorentz force term due to the presence of magnetic field. The magnetic field is acting only along the z-direction (i.e) $\boldsymbol{B}=\{0,0,B_z\}$. Since (3) and (4) are equations of 0^{th} order, the bandwidth of the problem is considerably reduced by substituting into (1). The substitution gives rise to convection-diffusion type equation, which apart from being more stable increases computational efficiency. After some algebraic manipulation, we end with the following equations,

$$\frac{\partial n_i}{\partial t} + b_i \left[\nabla.\left(n_i \mathrm{V}_i\right)_{B=0} - \mu_i^2 B_z \left\| J_{xy}\left(n_i, \varphi\right) \right\| \right] = \alpha \left| \Gamma_e \right| \tag{5}$$

$$\frac{\partial n_e}{\partial t} + b_e \left[\nabla.\left(n_e \mathrm{V}_e\right)_{B=0} - \mu_e^2 B_z \left\| J_{xy}\left(n_e, \varphi\right) \right\| \right] = \alpha \left| \Gamma_e \right| \tag{6}$$

where, $J_{xy}\left(n, \varphi\right) = \begin{pmatrix} \partial n/\partial x & \partial n/\partial y \\ \partial \varphi/\partial x & \partial \varphi/\partial y \end{pmatrix}$

Here $b_i(=1/1+\beta_i^2)$ and $b_e(=1/1+\beta_e^2)$ are functions of hall parameter (β_i and β_e) and ||J|| is the Jacobian determinant involving partial derivatives of n and φ.

In equations (5) and (6), the effect of magnetic field on the discharge is shown to have theoretically brought into the system through introduction of an additional expression involving mobility. The convective term ($\nabla.n\mu E$) gets altered accordingly in the x and y directions. This affects the coupling between the electric field and number density resulting in transfer of momentum between axes. An appropriate choice of B magnitude and direction can accordingly increase or decrease the stream wise momentum through electrostatic forces. Modification in discharge characteristics is expected in a direction perpendicular to the significant axis of the problem.

The electron mobility μ_e in Eqn (6) is given by[16] $\mu_e = 3\times10^6 cm^2 V^{-1} s^{-1}$, at *pd* = 0.2 Torr.cm. The electron diffusion coefficient, D_e is calculated from the Einstein relation $D_e = kT_e/e\mu_e$. The ion diffusion coefficient is $D_i = 2\times10^2 cm^2/s$ at 300K. The ion mobility μ_i is expressed as a function of reduced field *(E/p)*[6,17].

The relation between electrostatic field and charge separation is given by the Poisson equation

$$\varepsilon \nabla.\boldsymbol{E} = -e(n_e - n_i) \tag{7}$$

For pressure of 0.1 Torr in Argon; as low as <<1% of secondary electrons are emitted back from the electrode. Hence, the electrodes are assumed to be fully absorbing. Secondary Electron Emission (SEE) can be neglected

The system of equations (1)-(7) are normalized using the following dimensionless quantities:

$\tau = \omega t$, $z_i = x_i/d$, $N_e = n_e/n_0$, $N_i = n_i/n_0$, $u_e = V_e/V_B$, $u_i = V_i/V_B$ and $\phi = e\varphi/kT_e$ where $V_B = \sqrt{kT_e/m_i}$ is the Bohm velocity. For all the cases considered, d=2 cm, ω/2π=13.56MHz and the reference density $n_0 = 2\text{x}10^{15}\ \text{m}^{-3}$.

III. METHODOLOGY

The system of equations (1)-(7) is solved using a finite element formulation that has been described in our previous works[12-14]. The equations can be written using a linear operator in the form $L(\boldsymbol{q})=0$ where $\boldsymbol{q}$ is a vector of dependent variables, N_i, N_e *a*nd ϕ. For any admissible test function ψ, the discretized Galerkin Weak Statement (GWS) becomes

$$WS^h = S_e \left(\int_{\Omega_e} \left[\psi\, L(\boldsymbol{q})\, d\tau \right] \right)_e = 0 \tag{8}$$

over the non-overlapping union of all elements $\cup\Omega_e$. The time derivatives are evaluated using the fully implicit Euler method while the temporal evolution is explicit in nature. The nonlinear Newton-Rhapson scheme is used to solve the matrix using a Generalized Minimal RESidual solver to handle the sparseness of the resulting stiff matrix. The solution is assumed to have converged when the L_2 norm of all solution variables and residual are below a chosen convergence criterion ($\sim10^{-2}$). The system utilizes a Sub-Grid eMbedded algorithm (SGM)[13,18] for computational stability and control

of dispersion error. The SGM is incorporated to the dissipative flux terms that are altered suitably based on local cell velocity and is expected to ensure a node-wise monotone solution.

IV. RESULTS AND DISCUSSIONS:

A. One-Dimensional Discharge:

The system of equations (1)-(4) and (7) are solved for a preliminary one-dimensional geometry consisting of two electrodes one of which is grounded at zero potential while the other electrode is powered by an RF potential. The details of the geometry, boundary conditions and discharge parameters were reported earlier[5]. Here we present some representative results for the same.

Fig 1(i)-(ii) show the computed 1-D RF discharge characteristics for an applied frequency $\omega \approx 8.52 \times 10^7$ sec^{-1}. The distribution of electron gas in the gap between electrodes is periodic with applied frequency as shown in Fig 1(i). Depending on the instantaneous potential on the electrode, an anode or cathode sheath is formed in its vicinity. Fig 1(ii) shows the spatio-temporal evolution of the electrostatic field across the discharge gap. The nature of the field indicates the nature of electrodynamic sheath structure. The sheath thickness was correlated as $S_w \approx 0.04 \pm 0.03 \sin \omega t$ in the frequency of applied potential (ω). The simulation results predict the maximum sheath width as $S_{w\text{-}max} \sim 20\ \lambda_{De}$, which agrees with the available literature[19-20].

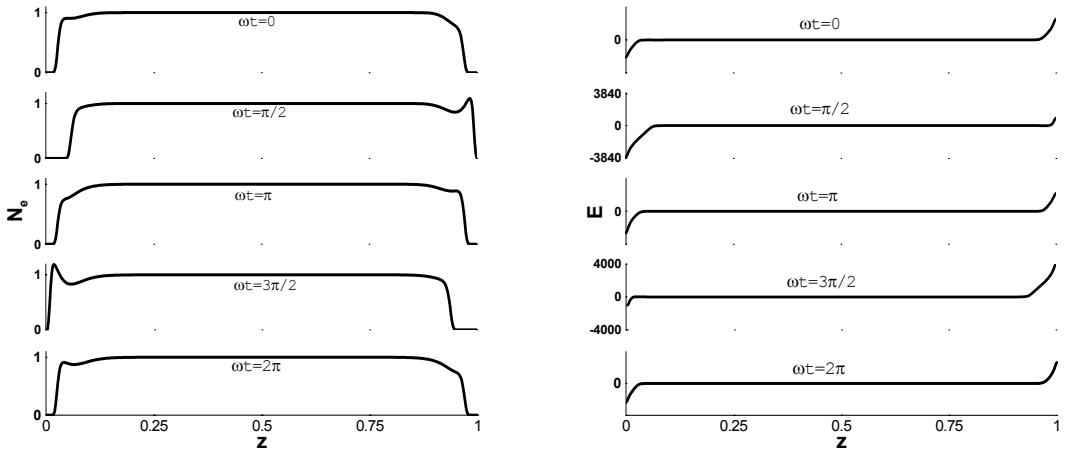

(i) (ii)

Figure 1: Spatio-temporal evolution of (i) electron number density, and (ii) electric field between electrodes in one dimension at various stations of a sinusoidal cycle (from Kumar and Roy, AIAA-2005-0948)

B. Two-Dimensional Discharge:

1. Benchmarking with nitrogen gas:

As the lateral extent of a discharge becomes comparable to the transverse stretch in presence of geometric or electrical inhomogeneities, the sheath becomes multi-dimensional and a one-dimensional model is not sufficient to capture the required features. Specifically, the interest to model the effect of magnetic field necessitates a higher dimensional consideration. First, the formulation is tested in two dimensions for plasma formed between two symmetric electrodes for a direct current glow discharge using nitrogen. The geometry and discharge conditions correspond to Surzhikov and Shang[10]. The computational grid consists of 25 x 30 bi-quadratic (9 node) finite elements. An electrode potential of 533 V is applied through an external circuit with resistance 300kΩ driven by an electromotive force of 2000 V. The model does not neglect diffusion in x and y directions for the entire domain including plasma and sheath.

The cathode is at y=0 while y=2 cm is the anode. Vanishing ion density is imposed at anode, the electrons at cathode are calculated from a flux balance using a secondary emission coefficient of 0.1. The left and right boundaries of the computational domain are maintained at symmetry conditions. Electrons and ions are concentrated near the center of the geometry along x-axis based on initial condition calculated based on a pre-estimated cathode layer thickness and current column length[10].

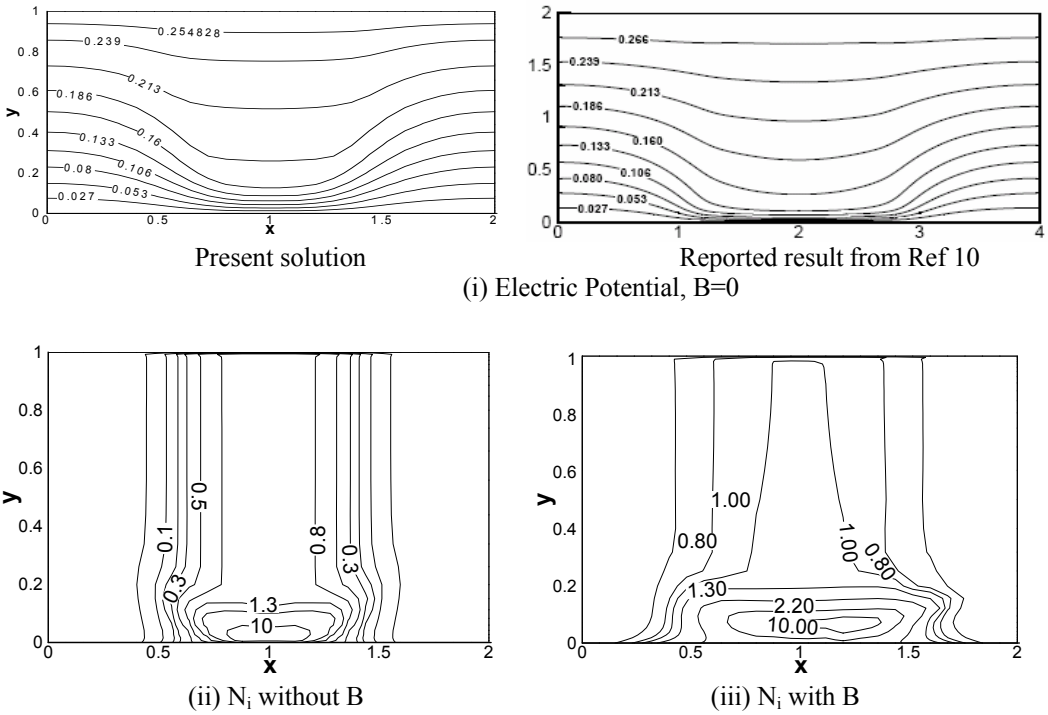

Present solution Reported result from Ref 10

(i) Electric Potential, B=0

(ii) N_i without B (iii) N_i with B

Figure 2. (i) Electric iso potential contours, (ii) Ion density contours for B=0 and (iii) Ion density contours for B=0.01 T. All results shown here are for nitrogen gas at 5 Torr.

The simulation results for electric potential and ion density at pressure of 5 torr with and without the magnetic field are presented in Fig 2. The computed potential is compared with results from Surzhikov and Shang[10] in Fig. 2 and is in good agreement. The potential lines bend towards the cathode. This gives rise to high electric field (directed towards the electrode) driving electrons away forming a cathode sheath thickness ~7.5 % of inter-electrode gap. The ion density near cathode rises to an order of magnitude higher than that near center of discharge channel and indicates a qualitative similarity[10]. When a magnetic field of 0.01 Tesla is applied, the ion density peak gets shifted in the axial direction along the electrode surface (Fig. 2(iii)). A widening of discharge near cathode is also observed. The direction of drift depends on direction of magnetic field lines while the magnitude of shift of iso-lines depends on value of determinant of equations (5) and (6).

2. Argon gas discharge:

The formulation thus calibrated with reported result is then applied to model plasma of a pure argon gas discharge. The schematic model and the computational domain are shown in Fig. 3. The electrode is 1.8 cm long and the leading edge is located 1.1 cm from left boundary. The top surface is considered quasi neutral. This assumption is valid as the height of domain chosen is much greater than electron debye length. A height of ~$200\lambda_{De}$ is chosen for present case. The electrodes are assumed to have a negligible thickness compared to the dimensions of the model and are ignored for simplicity in this case.

The computational grid (see Fig. 3) consists of 25 x 20 biased bi-quadratic finite elements with the first node ~0.01 cm away from wall. In the absence of magnetic field, the discharge may be treated as symmetric about x=1. Similar geometry has been treated recently in literature[9,11] for quiescent and fluctuating argon plasmas in the collisionless low-pressure regime. Apart from being a more realistic configuration that brings edge effects at the junction between the electrode and the insulator into consideration. The importance of understanding this discharge configuration proves useful in plasma based flow control application that is being widely investigated as a means to alter near wall boundary layer profile. A recent investigation studied the effect of plasma on neutral gas flow in an asymmetric configuration for a Dielectric Barrier Discharges (DBD)[21]. Hence this formulation provides a framework, which can be built upon to study high-pressure discharges and the effect of magnetic field interaction in collision-dominated sheath.

Note for this configuration in Fig. 3 below, there is a net flow of current into the metallic wall, while the current path is almost parallel to the dielectric surface. This gives rise to a near wall inhomogeneity in the model, which might be compared to a mathematical discontinuity. This inherent feature introduces considerable numerical difficulty at the electrode-insulator edge. Due to vast difference in potential across the insulator-conductor edge, maximum plasma

generation is limited to this region which when not properly handled may affect numerical stability. As mentioned earlier, artificial stabilization techniques like SGM have been implemented to minimize dispersion error and ensure numerical stability of the solution.

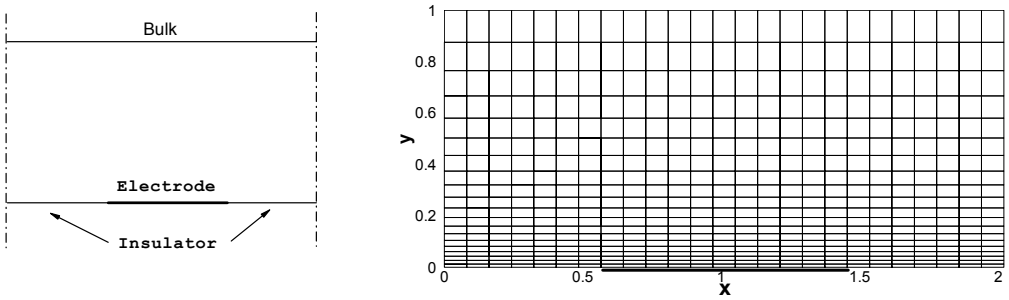

Figure 3. Schematic of a perfectly flat electrode-insulator configuration and computational grid.

For argon discharge, the system of equation (1)-(4) and (7) are solved for DC and RF applied potentials using the following boundary conditions. The electron flux imposed at electrode is based on the electron thermal velocity and directed towards the electrode. Electron flux normal to electrode is taken as zero if drift velocity is away from the electrode. Boundary condition (at electrodes) for ions is imposed homogeneous Neumann ($\partial N_i/\partial n=0$). The normal current of charge carriers is nullified at insulator boundary. In the left and right boundary, the slopes $\partial N_i/\partial x=0$, $\partial N_e/\partial x=0$ and $\partial \varphi/\partial x=0$ are enforced.

(a) DC Discharge:

A steady state discharge is first studied for an applied voltage of -50V on the exposed electrode. Fig. 4(i) shows the iso-lines of electric potential in two dimensions. The symmetric nature of the contour in the absence of magnetic field about x=1 may be noted. Figs 4(ii), (iii) and (iv) compare the axial distribution of potential, electron number density and charge difference close to the bottom plate. Due to large difference of potential between top boundary and electrode, the variation of characteristic is significant along the y-axis. The magnetic field strongly affects the stream-wise distribution because of high y-momentum transfer into the x-direction (as seen from Eq. (5) and (6)). The solid line shows the variation in absence of magnetic field while the dotted line is for a low magnetic field intensity of five Gauss. The sharp change of characteristics (for example, spike like pattern for electron number density) near the electrode-insulator edge is expected. Most of the plasma formation is limited to this region. As shown in Fig 4(ii), the insulator is less cathodic ($\sim 25V$ difference than cathode potential) and behaves like a pseudo-anode collecting electrons. Corresponding to this pseudo-electrode, a sharp increase in electron density is observed near the highly depleted cathode sheath layer. In the presence of magnetic field, the potential lines (for example, near right electrode-insulator edge) are affected along the electrode surface as they are shifted from its initial position towards the right. This change is reflected in the charged species (through the Poisson equation) causing a variation in charge separation.

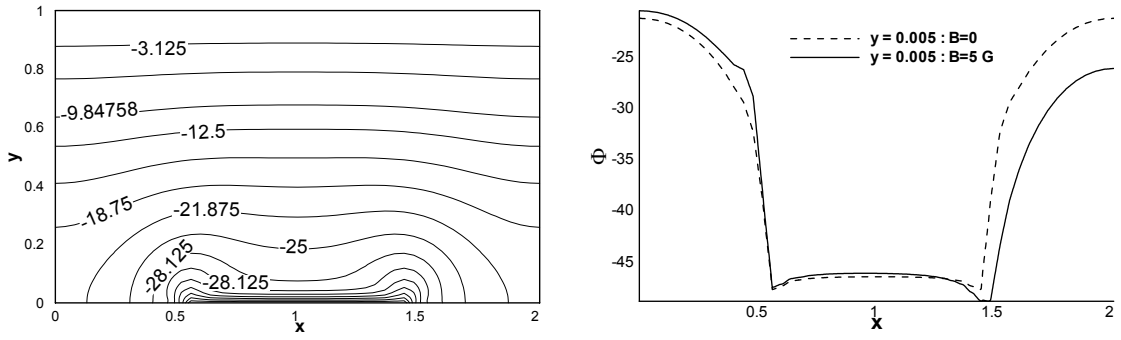

(i) (ii)

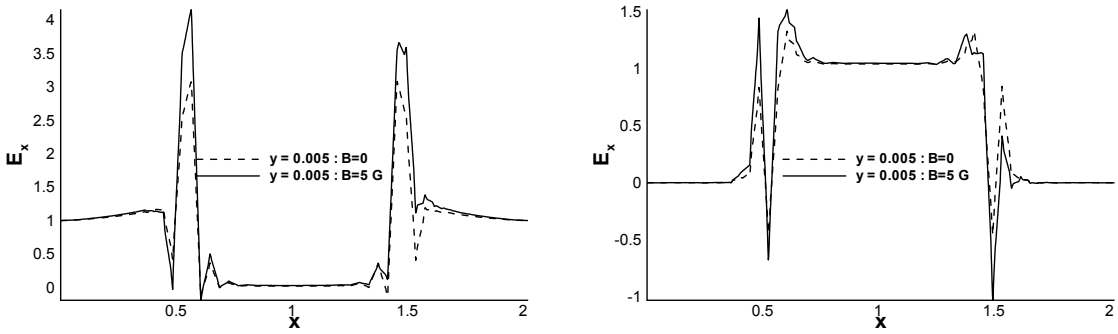

(iii) (iv)

Figure 4. Normalized solution for DC discharge (i) and (ii) Electric potential (iii) Electron number density and (iv) charge difference in the presence and absence of magnetic field. All results shown here are for argon at 0.1 Torr.

(b) RF Discharge:

The steady state discharge above was analyzed for fairly low magnetic field intensity. With the gained theoretical understanding of electromagnetic interactions, a transient plasma discharge is simulated for a higher magnetic field of 20 Gauss in the presence of an oscillating potential with a peak-to-peak of 100 volts. In order to understand the variation of plasma characteristics in the presence of magnetic field, the solution is compared with a simulation without the magnetic field, all other conditions being the same.

The streamwise and transverse variations at different locations are shown in Figs. 5 (i)-(iii). The results presented here are plotted along cuts in the vicinity of the edge for the negative half of the RF cycle. It was observed in the simulation that except for localized regions near the electrode-insulator edge, the magnetic field had less pronounced effect on the transverse solution characteristic relative to stream-wise components. This has been explained earlier from equations (5) and (6). There are some significant observations that can be made. The solid line plots streamwise and transverse variation in the presence of magnetic field against the dotted for no magnetic field. A ~60% shift of potential is noted near the left insulator-conductor edge between the two cases. The asymmetry is more prominent in the case of 20 Gauss field. Fig. 5(ii) shows electron number density close to the plate. In the presence of magnetic field, the electron drift velocities are altered and large electron accumulation (an order of magnitude higher than discharge center) is observed near one of the insulator-conductor edges. Fig. 5(iii) shows the variation of axial electric field near the insulator-conductor interface. The 20 Gauss field causes a 15 times increase in the near wall field.

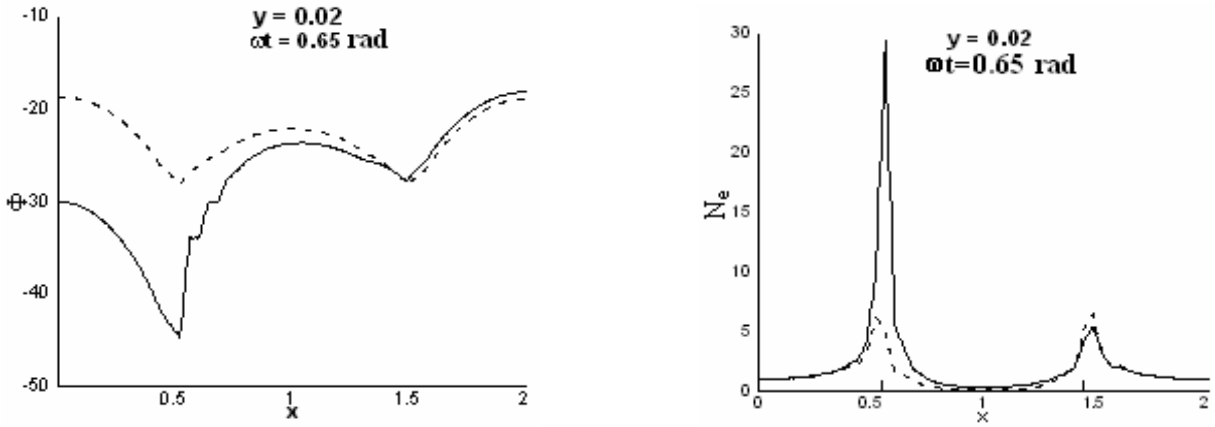

(i) (ii)

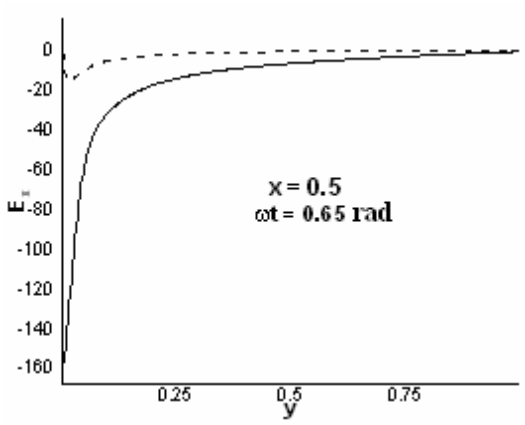

(iii)

Figure 5. RF discharge characteristics (i) Stream-wise potential along y=0.02, (ii) Electron number density contour along y=0.02 and (iii) Axial electric field along x=0.5. Solid line shows variation in presence of magnetic field of 20 Gauss. Dotted line is for B=0. All results shown here are for argon at 0.1 Torr.

C. Electrode shape effect

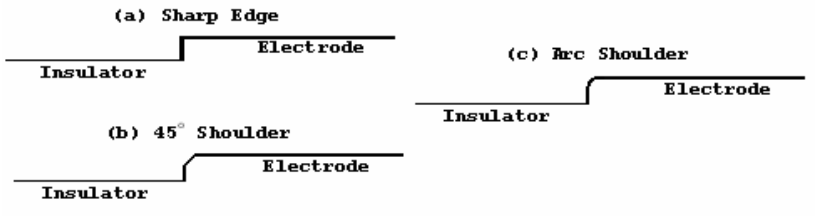

Figure 6. Electrode-insulator edge types

We have demonstrated that the presence of an insulator-conductor interface alters the nature of discharge and plays a significant role in altering electric forces due to plasma generation. The conductor in the previous case was assumed thin for simplicity in modeling. It has been shown recently that the shape of electrode plays a significant role in altering the nature of field lines and hence the "qE" forces near the wall[22]. To have an insight into this shape effect, two configurations, shown in Fig. 6(a) and (b) are investigated in the present study. The case of rounded edge (Fig. 6(c)) may be visualized as an intermediate case between 90^o and 45^o shoulder configurations.

For this study, we limit ourselves to a steady state in the absence of magnetic field for simplicity. The leading edge of an electrode of 0.2 mm thickness is located 1.5 cm from the left boundary. Fig. 6 (a) considers a sharp edge of electrode with a 90^o shoulder while Fig. 6(b) considers an edge with 45^o shoulder. The computational grid consists of 45 x 45 bi-quadratic finite elements in both cases. The discharge conditions are same as before, namely, 0.1 torr argon plasma with an electrode potential of –50V.

Fig. 7(i)-(iv) show the computed profiles for the above-mentioned cases. The region near the edge has been zoomed for clarity. From common understanding, the 90^o edge creates a sharp geometrical discontinuity resulting in abrupt change in radius of curvature across the edge as compared to the bevel. Hence, the spatial variation of electric field gets considerably modified altering the electrodynamic properties of the discharge between the two shapes. The electric field lines for a given change in potential are shown in Fig. 7(i)-(iv) and the effects are felt within few Debye lengths (*~0.1 cm)* into the plasma.

Fig. 7(v)-(vi) plots the force vector for the two shapes expressed as a product of space charge difference (N_i-N_e) and electrostatic field (E_x or E_y). In both cases, a strong electrostatic force in the positive x and negative y direction is noted close to the wall. The presence of cathode gives rise to strong transverse field (with electric field lines ending at cathode perpendicular to it) downstream of the edge. The direction of electric force vector (given by $\tan^{-1}(F_y/F_x)$) near the wall was predicted between 225^o to 260^o oriented mostly in the third quadrant. This is indicative of an effective forward-downward force created by the plasma across the edge. As compared to the beveled edge, the sharp 90^o corner with smallest radius of curvature shows ~22% increase in E_x and 15 % increase in E_y near the edge resulting in about the same percentage increase induced force components.

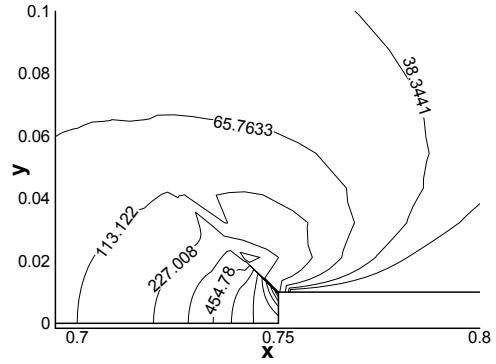

(i) E_x 90 degree

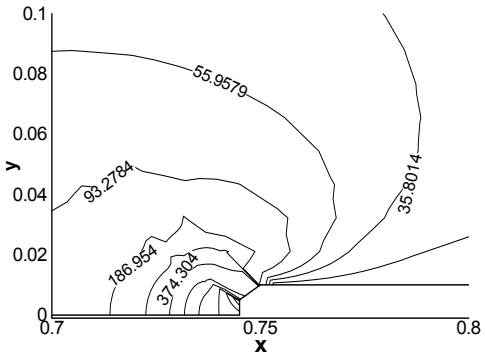

(ii) E_x 45 degree

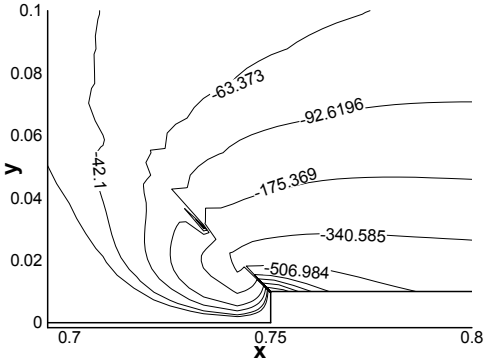

(iii) E_y 90 degree

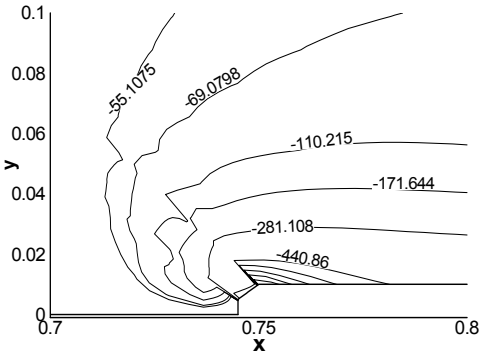

(iv)E_y 45 degree

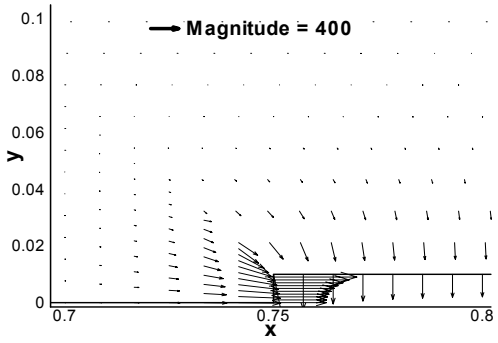

(v) F vector 90 degree

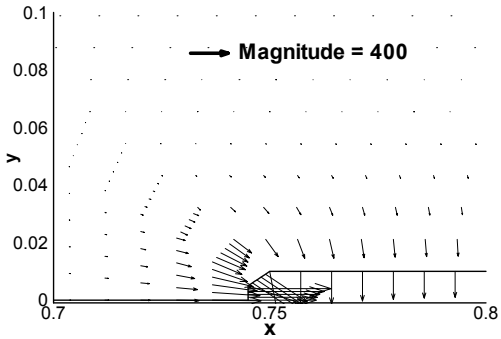

(vi) F vector 45 degree

Figure 7. Axial electric field (E_x), transverse electric field (E_y) and force vectors for 90^o shoulder and 45^o shoulder

V. CONCLUSIONS

We have presented a hydrodynamic model for a two-dimensional geometry driven by electric and applied magnetic fields. The equations of continuity, drift-diffusion along with electrostatic field equations are solved numerically using a self-consistent finite-element algorithm anchored in a Multi-scale Ionized Gas (MIG) flow code to simulate the plasma in the low-pressure regime under DC and RF potentials. The formulation was tested in two-dimension for plasma formed between two symmetric electrodes for a direct current glow discharge using nitrogen. The results match well with published literature. A steady state discharge is simulated for argon in an electrode-insulator configuration. The magnetic field has been shown to strongly affect the stream-wise distribution caused by the $\boldsymbol{V}\times\boldsymbol{B}$ coupling between x and y axes. Simulation results for a transient discharge evolution in the presence of time varying RF potential have been investigated. The present analyses have served to highlight the importance of understanding two-dimensional gas discharge nature and the effect of time varying potential and an external magnetic field on it. More rigorous treatment will follow in a future work. Finally, the shape effect in insulator-conductor configuration on near

wall dynamics is compared using a 90^o shoulder and 45^o chamfer. The maximum axial force is about ~22% higher for 90^o shoulder while the force vector across the edge indicates a net downward and forward force generated.

The potential of combined electric and magnetic fields as a productive means in altering near wall plasma forces has been realized here. The results presented are expected to help interpret the plasma formation in the presence electromagnetic interaction on the discharge structure for higher pressures. As a future effort, we also intend to correlate the plasma characteristics for varying magnetic field intensities.

REFERENCES:

[1] P. A. Miller and M. E. Riley, Journal of Applied Physics, 82(8), 3689 (1997).
[2]D. Bose, T. R. Govindan and M. Meyyappan, Journal of Applied Physics, 87(10), 7176 (2000).
[3]Y. Zhang, J. Liu, Y. Liu and X. Wang, Physics of Plasmas, 11(8), 3840 (2004).
[4]T. E. Nitschke and D. B. Graves, Journal of Applied Physics, 76(10), 5646 (1994).
[5]H. Kumar and S. Roy, 43rd AIAA Aerospace Sciences Meeting and Exhibit, AIAA-2005-0948.
[6]J. P. Boeuf, L. C. Pitchford, Physical Review E, 51(2), 1376 (1995).
[7]M. Dalvie, M. Surendra and G. S. Selwyn, Applied Physics Letters, 62(24), 3207 (1993).
[8]J. D. P. Passchier and W. J. Goedheer, Journal of Applied Physics, 74(6), 3744(1993).
[9]D. Kim and D. J. Economou, Journal of applied physics, 94(5), 2852(2003).
[10]S. T. Surzhikov and J. S. Shang, Journal of Computational Physics, 199, 437 (2004).
[11]L-J. Hou, Y-N. Wang and Z. L. Miskovic, Physics of Plasma, 11(9), 4456(2004).
[12]S. Roy and D. Gaitonde, Journal of Applied Physics, 96(5), 2476 (2004).
[13]S. Roy, B. P. Pandey, J. Poggie and D. Gaitonde, Physics of Plasmas, 10(6), 2578 (2003).
[14]S. Roy, and B. P. Pandey, Physics of Plasmas, 9(9), 4052 (2002).
[15]A. D. Richards, B. E. Thompson and H. H. Sawin, Applied physics letters, 50(9), 492(1987).
[16]L. Ward, Journal of Applied Physics, 33(9), 2789 (1962).
[17]I. D. Kaganovich, L. D. Tsendin and N. A. Yatsenko, Tech. Physics, 39(12), 1215(1994).
[18]S. Roy and A. J. Baker, Journal of Numerical heat transfer, 33(1), 5(1998).
[19]M. Lieberman, A. J. Lichtenberg, Principles of plasma discharges and material processing, John Wiley and Sons, Inc., 1994.
[20]Y. P. Raizer, M. N. Shneider and N. A. Yatsenko, Radio-frequency discharges, CRC Press, London, 1995.
[21]S. Roy, Applied Physics Letters, 86(10), 101502 (2005).
[22]C. L. Enloe, T. E. McLaughlin, R. D. VanDyken, K. D., Kachner, E. J. Jumper, T. C. Corke, M. Post, and O. Haddad, AIAA Journal, 42 (3) 595 (2004).